A NUMERICAL REPRESENTATION OF SELECTED EXPERIMENTAL STUDIES ON THE FAILURE LOAD CHARACTERISTICS OF REINFORCED CONCRETE BEAMS STRENGTHENED EXTERNALLY IN FLEXURE WITH STEEL PLATES

FRANCIS, E. W[1], [1]AUTA, S.M[1], AGUWA J.I, [1]ABDULLAHI, A

[1]Department of Civil Engineering, Federal University of Technology, Minna, Nigeria

Abstract

This study presents a numerical representation of selected experimental investigations on the failure-load behaviour of reinforced concrete beams strengthened externally in flexure with steel plates. The ABAQUS finite element software effectively reproduces key structural responses reported in the literature, including the initiation and propagation of cracks and the development of failure modes such as debonding and peeling. Validation of shear behaviour indicates that the model performs most accurately for beams with closely spaced stirrups, and its ability to capture diagonal compression (DC) cracking supports the conclusion of Oehlers (2001) that shear reinforcement cannot prevent the formation of initial cracks. Comparative analyses further show that beams with longer shear spans, such as those tested by Jones et al. (1982), are less susceptible to premature peeling, in contrast to short-span specimens reported by John et al. (2022). The numerical results clarify that peeling typically originates from flexural cracking at the plate-end, whereas debonding is governed by localized overstressing of weaker interfacial zones. Additionally, the study highlights the significant influence of plate thickness: reducing thickness decreases stiffness and load capacity, while excessive thickness can trigger premature failure in balanced or over-reinforced beams. Overall, the FE model demonstrates strong predictive capability and offers reliable insight into the mechanisms governing strengthened beam behaviour and associated failure modes.

Keywords: Failure Load, cohesive zone model, Strengthening, Premature failure, debonding; peeling

1.0 INTRODUCTION

Reinforced concrete (RC) beams are fundamental components in buildings, bridges, and other civil infrastructure systems [1]. With continued use, these beams often experience deterioration, increased service loads, or material aging that reduces their ability to safely sustain structural demands [2, 3]. When this happens, strengthening becomes necessary to restore or enhance their load-carrying capacity. Among the strengthening methods available, externally bonded steel plates remain one of the earliest and most practical techniques used in structural engineering [4, 5].

By bonding steel plates to the tension face of RC beams, the plates help carry additional tensile forces, delay cracking, and improve beam stiffness and ultimate load capacity [6, 7]. This technique is attractive because it is relatively easy to implement, cost-effective, and structurally efficient [8]. However, externally plated beams also face challenges such as premature debonding at the plate–concrete interface, anchorage failures, and altered failure patterns [9, 10, 11]. These issues highlight the need for a deeper understanding of how such strengthened beams behave at failure.

Over several decades, researchers such as Kamruzzaman [12], Sarhan [13], Obaydullah [14], Ebuka & TrustGod [15] and Ahmed [16] and have conducted numerous experimental studies to investigate the performance of RC beams strengthened with steel plates. Early studies showed significant improvements in flexural strength, but also revealed weaknesses associated with insufficient bonding and end-anchorage detailing [17. 18]. Later research explored variables such as plate thickness, adhesive type, surface preparation, mechanical anchorage, and failure mechanisms [19, 20, 21]. Across these studies, one key parameter remains central: the failure load. This is the maximum load the strengthened beam can carry before collapse or critical structural distress. Understanding how different strengthening configurations influence failure load is essential for improving design models and strengthening guidelines.

However, the findings from these experimental studies are often scattered across literature, presented under different testing conditions, and influenced by varying material properties. This makes it difficult to draw direct comparisons or extract unified conclusions. A numerical representation of selected experimental results provides a systematic way to organize these findings, reveal performance trends, and identify gaps in existing knowledge.

To further improve and validate this numerical representation, the present study employed ABAQUS finite element software. ABAQUS has been widely used in structural engineering research because of its ability to model nonlinear behaviour, simulate complex interactions such as the plate-to-concrete interface, and reproduce experimental failure mechanisms with high accuracy.

Therefore, this study seeks to numerically represent selected experimental investigations on RC beams strengthened externally in flexure with steel plates and to use ABAQUS to better understand the factors influencing failure load behaviour. This combined experimental-numerical approach provides a clearer basis for evaluating strengthening effectiveness and improving future design practices.

2.0 MATERIAL AND METHOD

CONSTITUTIVE MODEL OF REINFORCING BAR STEEL

Steel is assumed isotropic and exhibits elasto-plastic behavior in the numerical model. Reinforcing bars follow a bilinear stress-strain law, whereas the steel plates employ a trilinear model as recommended by the BS 8110-1:[22]. Shear stirrups were intentionally excluded, in line with Oehlers [23], who observed minimal effectiveness of shear reinforcement against diagonal compression cracking. The beams were designed to prevent shear failure, which is not regarded as premature for the purpose of this study.

At low strain levels, reinforcing steel behaves elastically, maintaining a constant stiffness defined by Young’s modulus. Plastic deformation begins at the yield point, where permanent strains develop alongside increasing elastic strains. Before yielding, deformation is fully recoverable; beyond yielding, the steel continues to carry load while accumulating permanent deformation and reduced stiffness.

The reinforcement bars and stirrups were assigned an elastic modulus of 200 GPa, a yield stress of 500 MPa, and a plastic modulus of 200 MPa. The external steel plates were modelled with an elastic modulus of 20 GPa, yield stress of 240 MPa, plastic modulus of 200 MPa, and Poisson's ratio of 0.3.

CONSTITUTIVE MODEL OF CONCRETE

Concrete's inelastic behavior was modelled using a combination of linear elasticity and nonlinear damaged plasticity, reflecting its limited capacity for deformation under applied loads. The linear elastic component captures the initial, recoverable deformation under low stress, while the nonlinear damaged plasticity accounts for permanent deformation and progressive deterioration under higher stress levels. This damaged plasticity model is particularly suitable for simulating concrete under a wide range of loading scenarios, as it incorporates the gradual reduction of stiffness in both tension and compression. As a result, it provides a realistic and accurate representation of concrete's mechanical response under different stress states.

i) Concrete Damaged Plasticity Model

A continuum-based plasticity model with damage effects was used to describe concrete behavior under both tensile and compressive loads. During uniaxial tension, the material exhibits a linear stress-strain response up to the tensile strength, ft_0. Once microcracking begins, the concrete no longer sustains higher loads, and stress gradually decreases with increasing strain, illustrating the softening process (Figure 1a).

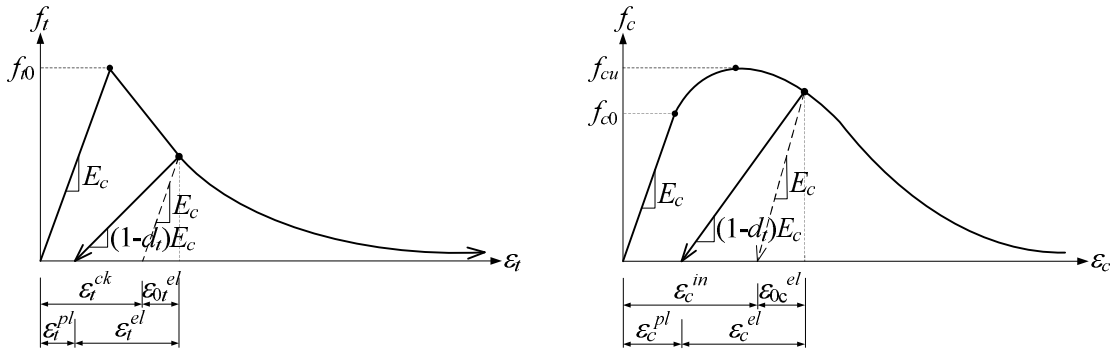

(a) (b)

Figure 1: Concrete damaged Plasticity model: (a)Tension Behaviour associated with tension Stiffening (b) Compressive Behaviour associated with Compressive Stiffening

In uniaxial compression, the behavior is also linear up to the initial yield point (fc_0). As the strain increases beyond this point, the stress rises to a peak value (fcu) in the plastic zone, after which the concrete undergoes strain softening, meaning the stress gradually decreases with further strain **(Figure 1b).** When unloading occurs from any point along the stress-strain curve, the remaining stress depends on the history of strain experienced, capturing the permanent damage in the material. Therefore, concrete stresses determined unloading from any point on the strain are given in Equations (1) and (2).

$$f_t = E_c\left(\varepsilon_t - \varepsilon_t^{pl}\right)\left(1 - d_t\right) \quad (1)$$

$$f_c = E_c\left(\varepsilon_c - \varepsilon_c^{pl}\right)\left(1 - d_c\right) \quad (2)$$

Where Ec is the modulus of elasticity of concrete. Then, the effective tensile and compressive cohesion stresses of concrete are estimated as shown in Equations (3) and (4).

$$\bar{f}_t = \frac{f_t}{\left(1 - d_t\right)} = E_c\left(\varepsilon_t - \varepsilon_t^{pl}\right) \quad (3)$$

$$\bar{f}_c = \frac{f_c}{\left(1 - d_c\right)} = E_c\left(\varepsilon_c - \varepsilon_c^{pl}\right) \quad (4)$$

Where:

$\tilde{f_t} = effective\ tensile\ stress$
$f_t = cracking\ strain\ in\ concrete$
$d_t = tensile\ damage\ variable$
$\in_t = total\ tensile\ strain$
$\in_t^{pl} = tensile\ plastic\ strain$

The post-failure behavior of reinforced concrete plays a critical role in determining the size and development of the failure surface, which is described in terms of post-failure stress as a function of cracking strain. Cracking strain represents the portion of total strain that exceeds the elastic limit, calculated as the total strain minus the elastic strain of undamaged concrete. This parameter is essential for defining tension stiffening behavior, which describes how the concrete between cracks continues to carry load after initial cracking. During unloading, and when the corresponding experimental or numerical data are available, ABAQUS automatically converts cracking strain into plastic strain using its built-in relationships [24]. This conversion allows the software to capture the irreversible deformation and energy dissipation associated with crack propagation. By accurately accounting for both the loading and unloading behavior, the model ensures a realistic representation of concrete's nonlinear response under cyclic and monotonic loading, improving the fidelity of the numerical simulations.

$$\varepsilon_t^{pl} = \varepsilon_t^{ck} - \frac{d_t}{\left(1 - d_t\right)}\frac{f_t}{E_0} \quad (5)$$

$$\varepsilon_c^{pl} = \varepsilon_c^{ck} - \frac{d_c}{\left(1 - d_c\right)}\frac{f_c}{E_0} \quad (6)$$

Where:

$\in_c^{pl} = plastic\ strain\ in\ concrete$
$\in_c^{ck} = cracking\ strain\ in\ concrete$
$d_c = concrete\ damage\ parameter$
$f_c = compressive\ stress\ in\ concrete$
$E_0 = initial\ (undamaged)\ elastic\ modulus\ of\ concrete$

The constitutive model's concrete and steel properties were derived from experimental results reported by Jones et al. [25]. From 28-day cylinder tests, the concrete's compressive yield strength (fc) was 32.3 MPa, and the ultimate compressive strength (fcu) was 39.2 MPa. Its Young's modulus (Ec) was 28.3 GPa, and the Poisson's ratio (νc) was 0.19. The tensile strength (ft_0) was estimated using the formula ft_0=0.6fcu, resulting in 3.76 MPa.

To simulate the concrete behavior more accurately, the concrete damaged plasticity model was used in ABAQUS. However, regions of the mesh without reinforcement tend to deform excessively under tension. To avoid this, the tensile post-failure behavior was defined using a fracture energy-based cracking criterion, represented by a stress vs displacement curve rather than a stress vs strain curve, as shown in Figure 2(a). The loss of stiffness due to tensile cracking, denoted as damage variable *dt*, is shown in Figure 2(b), with no recovery in compression (compression recovery factor = 0). To better represent the post-failure tensile behavior, the tensile stresses from the ABAQUS manual were scaled by a factor of 1.253. For compressive crushing, a stiffness degradation of 50% (damage variable *dc*) was assumed at a strain of 0.0014, and a tension recovery factor of 0.8 was applied.

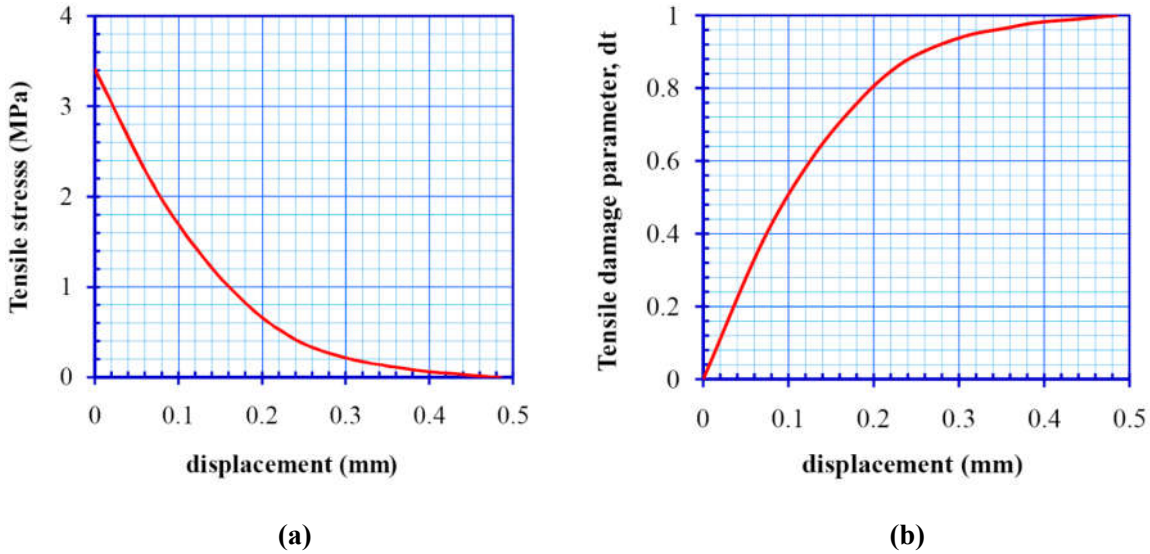

Figure 2. Post-failure stiffness degradation and damage properties of concrete: (a) Stress–displacement relation; and (b) Tension damage model

3.4.1.3 Adhesive Layer

A traction-to-separation approach based on the Cohesive Zone Model (CZM) was adopted to simulate the adhesive interface, ensuring consistency with experimental results and literature benchmarks. To model interfacial cracking, cohesive elements were inserted along the critical Crack 5 region, identified through prior studies (Figure 3). Unlike previous models by Adhikary and Mutsuyoshi [26] and Ziraba and Baluch [27], which assumed a brittle, linear elastic bond, this study applies a mixed-mode cohesive material model. The bilinear stress-strain relationship captures both the adhesive behavior and crack evolution: the interface responds elastically until damage initiation, after which damage progresses linearly until complete separation, as illustrated in Figure 3.

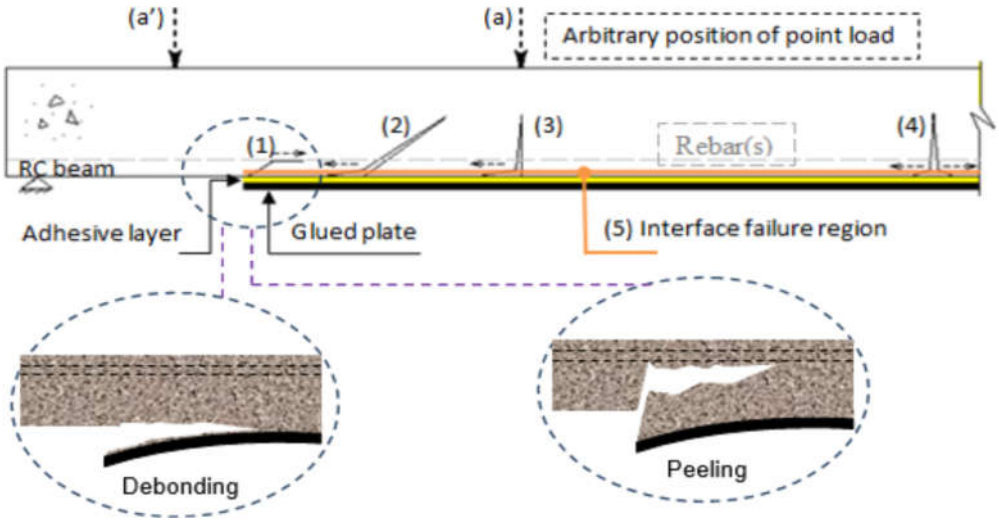

Figure 3. *Premature failure modes observed on the soffit of a plated RC beam under an arbitrarily positioned point load. The modes include: (1) peeling; (2) diagonal tension cracking (DC); (3) flexural cracking (FC); (4) pure flexural cracking (PFC); and (5) interface cracking and debonding.*

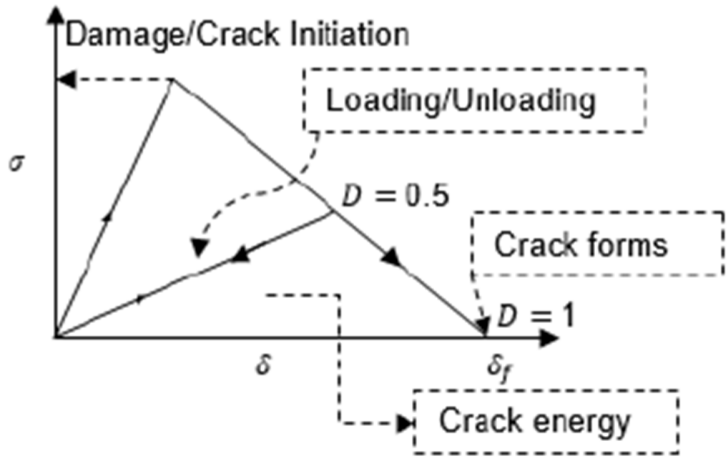

Figure 4. *Linear damage behaviour for the cohesive element as implemented in Abaqus.*

The adhesive layer is assigned a Poisson's ratio of 0.16, based on Ziraba and Baluch [27]. A damage parameter, denoted as D_m, tracks the degradation of the cohesive elements from 0 (no damage) to 1 (complete failure). This is governed by a damage evolution rule, given by (7),

$$D_m = \begin{cases} 0, & \delta_m \le \delta_m^{\circ}, \\ \dfrac{\delta_m^f(\delta_m^{\max} - \delta_m^{\circ})}{\delta_m^{\max}(\delta_m^f - \delta_m^{\circ})}, & \delta_m^{\circ} < \delta_m < \delta_m^f, \\ 1, & \delta_m \ge \delta_m^f, \end{cases} \tag{7}$$

where t_m is the mixed-mode stress and δ_m is the mixed-mode displacement. Once δ_m reaches or exceeds a critical displacement $\delta^f m$, D_m becomes 1 and t_m drops to zero indicating that the interface can no longer transfer any stress.

Earlier observations by Ascione and Feo [28] showed that, in addition to high transverse stresses, notable normal stresses can develop near but not exactly at the plate end, potentially leading to cracking. Building on their findings, the current study includes both normal and transverse bond interactions to more accurately model the failure behavior near the plate ends.

3.4.2 *FE model*

Numerical simulation of reinforced concrete structures requires an accurate representation of both the structural elements and their composite nature, combining concrete and steel. In this study, each section of the beam was first sketched individually in ABAQUS and then extruded to form a 3D solid model.
To simulate the beam's mechanical response, a deformable solid element type was adopted. The concrete was represented using an 8-node continuum solid element, which provides three translational degrees of freedom at each node along the x, y, and z axes. This element is suitable for modeling plastic deformation, cracking in three orthogonal directions, and crushing, thereby enabling a comprehensive representation of the concrete's complex behavior under loading.

To enable proper load application and efficient meshing, the concrete beam (2250 × 130 × 100 mm) was partitioned as required. The study utilized a 3D nonlinear finite element analysis, verified against theoretical predictions and validated with experimental results from the literature. Crack propagation was the primary focus, and a 3D plane stress approach was applied. Simulations were performed in ABAQUS 6.14 on a Windows operating system using a nonlinear static procedure solved with the full-Newton method. Quadratic continuum elements with reduced integration (CPS8R) were used for concrete and steel, while the adhesive layer was modeled with four-noded 3D cohesive elements (COH2D4).

To ensure consistency in behavior and compatibility, the steel plate and the equivalent rebar sections are assigned elements of matching sizes. A finer mesh is applied to the cohesive layer particularly in the regions where cracks are expected to form with a base element width of one unit to improve accuracy in capturing crack propagation.

Loading and Boundary Conditions: To simplify the analysis and reduce computational effort, only half of the beam is modelled, taking advantage of symmetry along the y-axis at the mid-depth of the section. Support plates are included beneath the beam to prevent punching under the applied loads and to allow free rotation at the supports. To minimize stress concentrations and avoid numerical instability, a finer mesh is used around the support and load plates. Instead of applying forces directly (as done in MLT-2), loads are introduced through prescribed displacements at the load plates. This approach significantly shortens the analysis time.

To ensure accuracy, the load application is controlled using incremental steps. The initial load increment is set to 10^{-5}, while the maximum allowed increment is 10^{-2}. These settings help strike a balance between solution precision and computational efficiency.

Concrete and Steel: In the models developed for the specimens tested by Jones et al. [27], the

total number of nodes and elements used were 4,352 nodes and 1,715 elements for the plated beam, and 1,917 nodes and 584 elements for the unplated beam. Similarly, for another set of specimens by Jones et al. [27], the models included 5,065 nodes and 1,957 elements for the plated section, and 2,575 nodes and 800 elements for the unplated section. In practical situations, cracks or debonding between materials do not occur due to perfectly clean separation between the two interfaces. Instead, the failure tends to occur near a perfectly bonded state. Based on this understanding, a perfect bond was assumed between the reinforcing steel and the surrounding concrete in the numerical models. Any cracking or damage in the materials was captured through their respective constitutive models.

Adhesive: The cohesive elements are arranged horizontally and connected to the concrete elements above and the steel plate elements below using a surface-to-surface interaction method with discretization. The Cohesive Zone Model (CZM) is used as a versatile approach to define the adhesive layer's geometry specifically its width and thickness as well as to specify the material properties of the adhesive and/or concrete, along with the characteristics of the crack behavior.

2.4.1. *Mesh sensitivity*

Due to differences in cross-sections between plated and unplated beams, mesh verification was conducted using a plated beam to match the study's focus. Beam URB4 from Jones et al. [27], with a balanced cross-section, was chosen for this purpose, while other beams, including unplated types, were employed for cross-checking and validation. Changes in element size affect concrete's tensile fracture energy (Equation 6). Even when fracture energy is kept constant, increasing the element width (b) spreads the cracking strain or energy over a larger area (b × thickness), thereby increasing the beam's load capacity. Figure 5 shows step by step modelling of plated reinforced concrete beam using Abaqus.

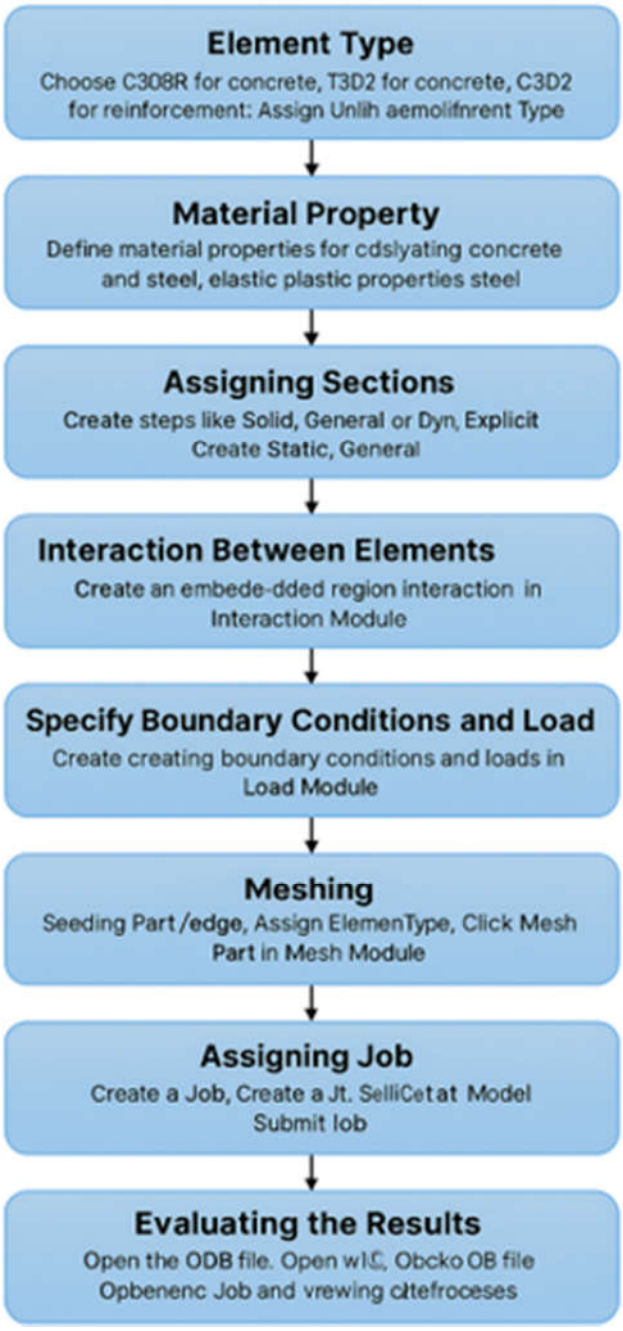

Figure 5. Flow Chart for a complete Abaqus Analysis

3.0 RESULTS AND DISCUSSION

Considering the intension of the research, the availability of information, and the broad range of research in this area, numerical representation was carried out using beams reported by Jones et

al. [27] and John et al. [29].The selected specimens represent a wide range of parameters, including variations in beam dimensions, material properties, shear span-to-depth ratios, adhesive thicknesses, plate thicknesses and lengths and the different failure modes observed in practice.

3.1 Specimens of John et al. [29]

The experimental research by John et al. [29] involved thirteen RC beams, consisting of one control beam (PA_O) and several strengthened specimens retrofitted with 1.0 mm, 1.5 mm and 2.0 mm thick steel plates using four different adhesive bond thicknesses of 2 mm, 4 mm, 6 mm and 8 mm applied to the tension face. All beams were tested as simply supported members. For numerical representation, four representative beams, PA_O, PFA_1.0, PFB_1.5 and PFC_2, were selected.

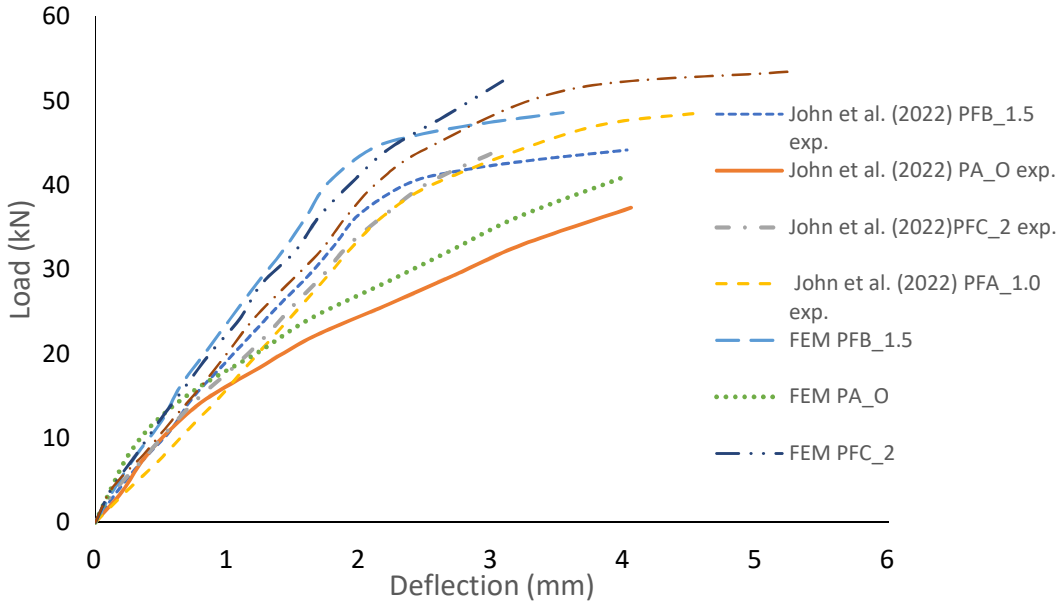

Figure 6: Load versus deflection graph

The load–deflection behaviour presented in Figure 6 shows clear differences among the beams in terms of failure load, stiffness, and energy absorption. PFB_1.5 develops the highest failure load of about 50–55 kN, followed closely by PFC_2 at 48–52 kN and PFA_1.0 at around 45–48 kN, while PA_O records the lowest capacity at 35–38 kN. The FEM predictions follow the same hierarchy (PFB_1.5 > PFC_2 > PFA_1.0 > PA_O), although they slightly underestimate peak loads at larger deflections due to conservative modelling assumptions. In terms of stiffness, PFB_1.5 again shows the steepest initial slope and therefore the highest stiffness, with PFC_2 behaving similarly in the early loading stages; PFA_1.0 displays moderate stiffness, while PA_O has the lowest, shown by its flat initial gradient. The FEM stiffness trends match the experimental data, with close agreement in the elastic region and divergence as cracking progresses. Energy absorption, reflected by the area under the curve, is also greatest for PFB_1.5, which sustains high loads over large deflections and exhibits strong ductility. PFC_2 follows with similarly post-peak behaviour, while PFA_1.0 shows moderate energy absorption and PA_O the least, owing to its lower peak load and smaller curve area. FEM predictions capture these trends but slightly

underestimate ductility due to simplified material representation. Overall, PFB_1.5 consistently demonstrates superior strength, stiffness, and energy absorption, while PA_O performs poorest across all parameters, and the FEM results reliably reproduce the observed experimental behaviour.

The behaviour of the beams further illustrates a clear pattern of progressive damage, characterized by the initiation and development of several key failure mechanisms. As loading increased, early flexural cracks formed in the tension zone, gradually widened and propagated toward the neutral axis. This was followed by localized plate-end debonding, where separation between the bonded plate and the concrete surface began to occur due to high interfacial stresses. With continued loading, this debonding extended along the plate length, leading to noticeable peeling of the external plate from the concrete substrate. These effects were accompanied by concentrated cracking around the regions of maximum bending moment and near the plate ends. This sequence of damage modes, as shown in Figure 7, demonstrates the progression of failure in the strengthened beams under increasing load.

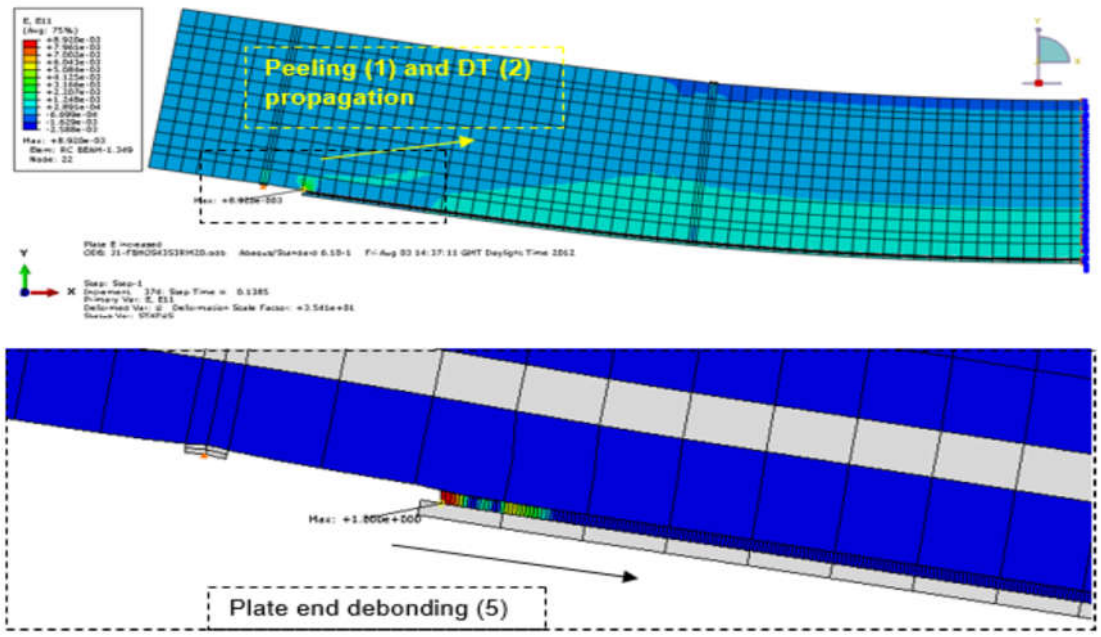

Figure 7: Capturing plate-end debonding, peeling and tension

3.2. Specimens of Jones et al. [1982]

The laboratory study by Jones et al. [27] involved eight reinforced concrete beams, of which three were under reinforced including the control beam URB1, one beam URB4 had balanced reinforcement, and the remaining beams were over reinforced using externally bonded plates. Four representative beams URB1, URB2, URB4 and URB5 were selected for comparison with finite element model (FEM) predictions.

Figure 8 show that the FEM generally aligns well with experimental results, particularly in capturing the overall load strain behaviour of both rebars and bonded steel plates. In the elastic

range, the FEM tends to predict slightly lower strain values, indicating conservative stiffness estimates. As loading increases, FEM models with thinner plates sometimes show higher stiffness than observed experimentally, while near failure the numerical response gradually softens.

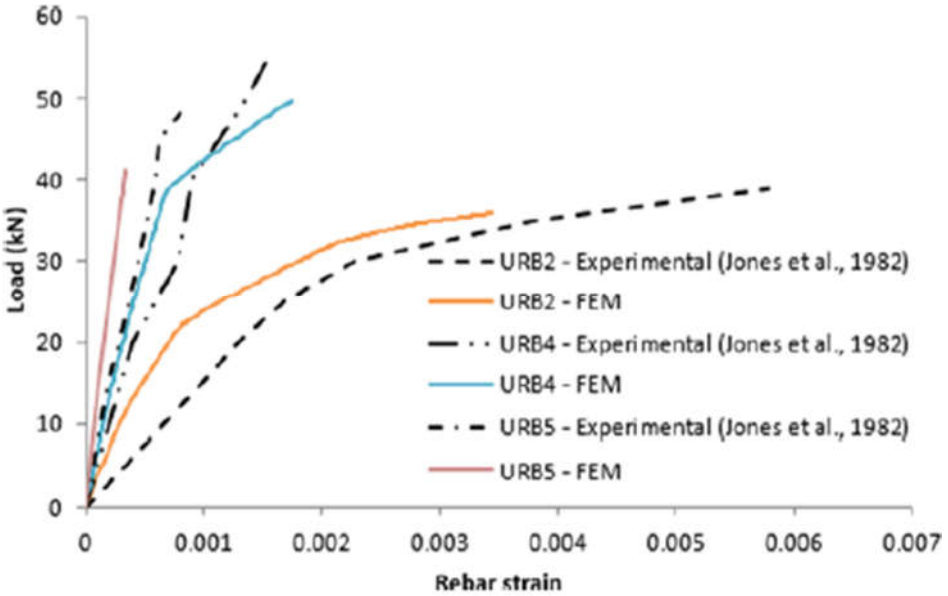

(a)

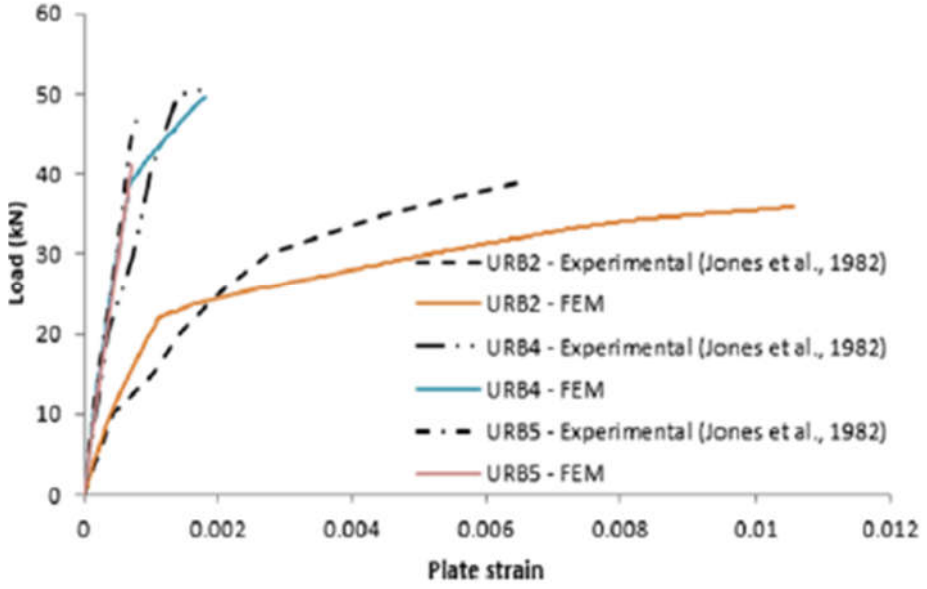

(b)

Figure 8: (a) Load versus strains in rebar; and (b) Load versus strains in rebar

Some discrepancies arise across specimens. For URB2, the FEM predicts higher plate strains at lower loads. For URB4, FEM and experimental results agree reasonably well up to moderate loads, though FEM slightly overestimates stiffness at higher loads. For URB5, the experimental beams

exhibit higher strains at lower loads, while the FEM predicts a stiffer response and higher load capacity.

These deviations primarily result from modelling assumptions such as perfect bond between steel and concrete, simplified adhesive behaviour, and idealized material models that do not fully represent bond slip, micro cracking, strain localization, or nonlinear failure mechanisms. Experimental factors including strain gauge placement, shear lag, residual stresses, and load imperfections also contribute. Overall, while the FEM effectively captures global behaviour, experimental beams display more ductile and strain sensitive responses due to the complex real interactions between materials.

The finite element results clearly captured the development of flexural cracks and a typical flexural failure mode, which aligns well with the experimental observations reported by Jones et al. [27]. The predicted failure loads and mechanisms including reinforcement yielding and mid-span debonding were consistent with those documented in the literature. As illustrated in Figure 8, the cracks initiated at mid-span and gradually spread outward as the load increased, reflecting the progression of flexural damage.

The behaviour of the balanced and over-reinforced beams was different. For these specimens, failure was dominated not by flexural cracking but by debonding at the plate ends. The crack patterns shown in Figure 8 emphasize this distinction: while URB2 exhibited cracks radiating outward from the beam's center, the strengthened beams tended to fail through premature debonding near the edges of the externally bonded plates.

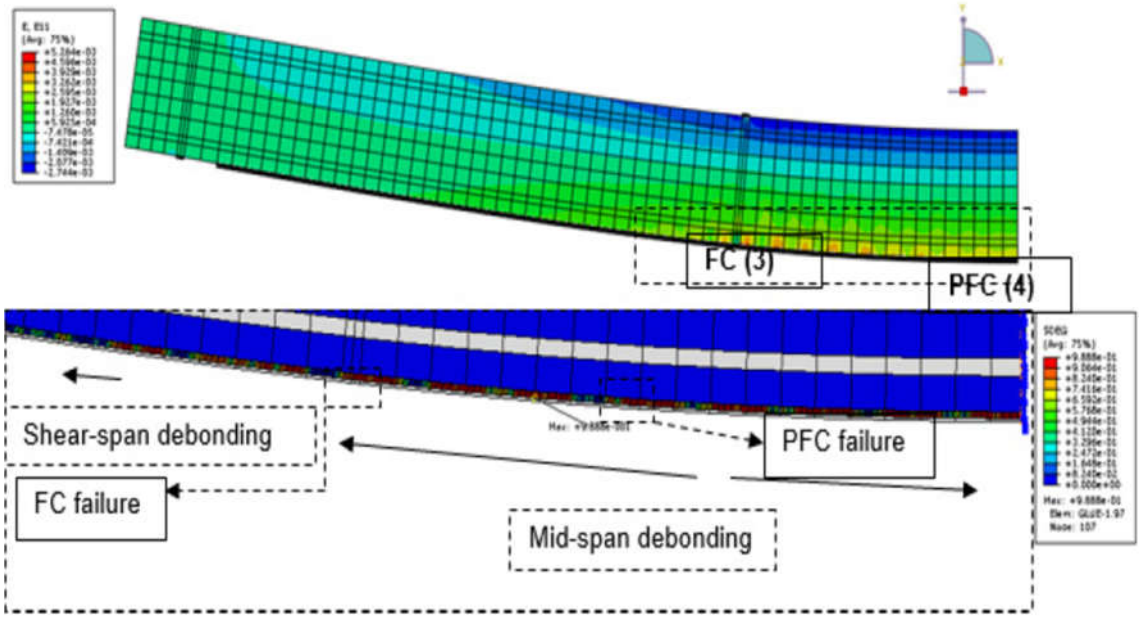

Figure 9: Showing FC cracks pattern (beam URB2)

4. CONCLUSIONS

The FE model demonstrates a high level of accuracy when compared with findings from previous experimental and analytical studies, effectively reproducing the sequence of crack initiation, propagation and the subsequent progression toward failure mechanisms such as debonding and peeling. In terms of shear behaviour, the model shows the strongest agreement with beams containing closely spaced stirrups, as these specimens provide clearer and more predictable crack patterns. Its ability to capture the formation of diagonal compression cracks also reinforces the conclusion made by Oehlers [23], who argued that shear reinforcement does not prevent cracks from forming but instead helps control their width and distribution.

The comparisons further reveal that beams with longer shear spans, such as those investigated by Jones et al. [27], tend to experience less premature peeling. This contrasts with the behaviour of short-span beams tested by John et al. [29], where the combination of high shear forces and abrupt stress transfer near the plate ends makes the system more vulnerable to early peeling failures. With regard to failure modes, the results consistently show that peeling usually initiates from a flexural crack located near the plate end, where high interfacial stresses develop. Debonding, on the other hand, is closely associated with weaker or imperfect interfacial zones that gradually become overstressed as loading increases.

The study also verifies the significant influence of plate thickness: thinner plates reduce overall stiffness and strength, while excessively thick plates can induce premature failure in balanced or over-reinforced beams. Overall, the FE model successfully mirrors the critical crack patterns and failure behaviours observed experimentally, providing strong confidence in its reliability.

Reference

[1] Luchko, J., Nazarevich, B., & Kovalchuk, V. V. (2022). Degradating Concrete and Reinforced Concrete Building Structures and Long-Term Structures. Bulletin of Odessa State Academy of Civil Engineering and Architecture, No. 86 (2022), pp. 35–46. 10.31650/2415 377x-2022-86-35-46.

[2] Shengyuan Li, Henglin Lv, Tianhua Huang, Zhigang Zhang, Jin Yao & Xin Ni (2022) Degradation of Reinforced Concrete Beams Subjected to Sustained Loading and Multi-Environmental Factors. Buildings 2022, 12(9), 1382; https://doi.org/10.3390/buildings12091382.

[3] Al-Mortadha, O. A., & Sultan A. D. (2024). Flexure Behaviour of Corroded Reinforcement Concrete Beams Under Sustained Loads, Civil and Environmental Engineering, 20 (2) pp. 1162 – 1173. https://doi.org/10.2478/cee-2024-0085.

[4] Shatha, A., Payam S., & Zainah I., (2020). Experimental Study on the Flexural Behavior of over Reinforced Concrete Beams Bolted with Compression Steel Plate: Part I. Applied Sciences, 10(3), 822; https://doi.org/10.3390/app10030822

[5] John A. T., Osuji S. O., & Nwankwo E. (2022) Determination of Optimum Bond Thickness of Reinforced Concrete Beam Strengthened Externally by Bonded Steel Plates. Umudike Journal of Engineering and Technology (UJET), 8 (1), pp. 23 – 36.

[6] Qin, Z., Tian, Y., Li, G., & Liu, L. (2019). Study on bending behaviors of severely pre-cracked RC beams strengthened by BFRP sheets and steel plates. Construction and Building Materials, 219, 131-143.

[7] Ibrahim, K. M., & Aziz A. (2025). Finite element modelling of RC beam strengthened with epoxy-bonded steel plate. Journal of Building Pathology and Rehabilitation 11(1), doi.org/10.1007/s41024-025-00672-y.

[9] Khan, M. A., El-Rimawi, J., & Silberschmidt, V. V. (2017). Relative behaviour of premature failures in adhesively plated RC beam using controllable and existing parameters. Composite Structures, 180, 75-87.

[10] Esmaeili, J., Aghdam, O. R., Andalibi, K., Kasaei, J., & Gencel, O. (2022). Experimental and numerical investigations on a novel plate anchorage system to solve FRP debonding problem in the strengthened RC beams. Journal of Building Engineering, 45, 103413.

[11] Chole, A., Tembhurne, A., Bawanthade, A., Bhadade, H., Khan, H. A., & Shaw, S. K. (2023). Strengthening of reinforced concrete beams by using FRPs-An overview. Materials Today: Proceedings.

[12] Kamruzzaman, M. (2017). Mitigation of Plate end Debonding in CFRP Strengthened Wide-Flange Steel I-Beams under Monotonic and Fatigue Loading (Doctoral dissertation, University of Malaya (Malaysia)).

[13] Sarhan, M. M. (2019). Flexural Behaviour of Concrete Beams Reinforced with Steel Plates (Doctoral dissertation, University of Wollongong).

[14] Obaydullah, M. (2021). Strengthening of Prestressed Concrete Beams Using Combined Externally Bonded and Prestressed near Surface Mounted Technique (Doctoral dissertation, University of Malaya (Malaysia)).

[15] Ebuka, N., & TrustGod J. (2023) Theoretical and experimental assessment of the effect of adhesive bond thickness on the flexural capacity of CFRP strengthened beams. CTU Journal of Innovation and Sustainable Development, 15(2), 139-147

[16] Ahmed Ibrahim, O. (2025). Enhancing Composite Steel-Concrete Beams: A Review of Strengthening Techniques, Performance, and Practical Applications. ERU Research Journal, 4(4), 3336-3356.

[17] Wang, Q., Zhu, H., Zhang, B., Tong, Y., Teng, F., & Su, W. (2020). Anchorage systems for reinforced concrete structures strengthened with fiber-reinforced polymer composites: State-of-the-art review. Journal of reinforced Plastics and Composites, 39(9-10), 327-344.

[18] Makhlouf, M. H., & Mansour, M. H. (2023). Efficiency of innovative strengthening techniques and anchorage systems using different materials on flexure performance of RC beams. Case Studies in Construction Materials, 18, e01733.

[19] Moore, C. M. (2019). A study on end-anchorage and bond behavior of steel-fiber reinforced cementitious matrix composites externally bonded to a concrete substrate. Missouri University of Science and Technology.

[20] Ryan, P. J. (2022). Detailing of Carbon Fiber Reinforced Polymer Anchorage for Shear Strengthening.

[21] Makhlouf, M. H., El-Azab, I. A., & Mansour, M. H. (2024). Flexural improvement of RC slabs by FRP or steel using different strengthening systems and novel anchoring techniques. International Journal of Concrete Structures and Materials, 18(1), 45.

[22] BSI (1990). BS 8110-1:1990. Structural use of concrete – Code of practice for design and construction. London: British Standards Institution.

[23] Oehlers, D. J. (2001). "Development of design rules for retrofitting by adhesive bonding or bolting either FRP or steel plates to RC beams or slabs in bridges and buildings." Composites Part A: Applied Science and Manufacturing, 32(9), 1345–1355. 10.1016/S1359-835X(01)00089-6

[24] ABAQUS/Explicit, (2004), Theory Manual, Version 6.4.1, Hibbitt Karlsson & Sorensen, Inc., USA.

[25] Jones, R., Swamy, R. N., and Ang, T. H. (1982), "Under- and Over-reinforced Concrete Beams with Glued Steel Plates", The International Journal of Cement Composites and Lightweight Concrete, 4(1), pp 19-32.

[26] Adhikary, B. B., & Mutsuyoshi, H. (2002). Numerical simulation of steel-plate strengthened concrete beam by a non-linear finite element method model. Construction and Building Materials, 16(5), 291-301.

[27] Ziraba, Y. N. and Baluch, M. H. [1995] "Computational model for reinforced concrete beams strengthened by epoxy bonded steel plates," Finite Elem. Anal. Des. 20, 253–271.

[28] Ascione, L. and Feo, L. [2000] "Modeling of composite/concrete interface of RC beams strengthened with composite laminates," Compos. B, Eng. 31, 535–540.

[29] John, A. T., Osuji S. O., Nwankwo, E. (2022a). Carbon Fiber Reinforced Polymer Surface Area and Bond Thickness Variation in Shear Strengthening of Reinforced Concrete Beam. SSRG International Journal of Civil Engineering, 9 (3), pp. 14-23. 10.14445/23488352/IJCE-V9I3P102